Strata deformation above a longwall coal mine

CSIRO

June 15, 2017

Contents

1 Introduction

In an underground longwall coal mine, coal is mined in "panels", as shown in Figure 1.1. These panels are typically 3–4 m in height, 150–400 m in width and 1000–4000 m long. Coal is extracted from one end, moving towards the other end. As mining progresses, a void is created behind the mining machinery where the coal used to be. The rock material above this void — the "overburden" – is not strong enough to support itself, so it collapses downwards. The resulting partial void and collapsed material is called the "goaf" (or "gob").

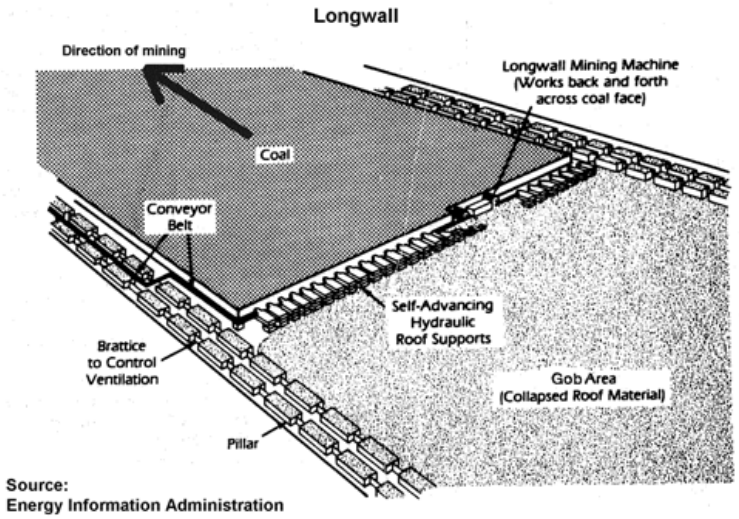

Figure 1.1: Pictorial representation of a single panel in longwall mining. The dimensions and process are described in the text. Figure sourced from citizensagainstlongwallmining.org who obtained it from the Energy Information Administration.

There are many geotechnical aspects that are of interest in this process, but this Example concentrates on the following.

1. The vertical displacement of the ground surface due to the longwall mining. This is called the "subsidence". This obviously has effects on buildings and other man-made structures like roads, but it can also change surface water pathways, affect vegetation, and cause surface-water ponding, which all have effects on the local ecology.

2. The vertical deformation within the overburden.

3. The patterns of fracture in the overburden. Together with Item 2, this can have effects on operational aspects of longwall mining, such as the load patterns on the "chocks" that support the roof of the goaf next to the mining machinery. It also strongly effects the flow of fluids in the porous rocks that make up the overburden. If the fracturing and deformation is extensive then fluids can easily move through the rock. This can result in mines flooding with water, or causing excessive drawdown of groundwater aquifers which can effect other users of groundwater (such as irrigators for farming) or can effect the rates of groundwater baseflow to surrounding river systems which may effect local and not-so-local ecosystems. The deformation and fracture of the overburden can also lead to aquifer mixing, where an aquifer consisting of "dirty" water (with high salinity, for example) pollutes a nearby aquifer of clean water. The deformation and fracture can also lead to large releases of methane gas from overlying (and underlying) coal seams. This methane can then flow through the highly permeable fractured rock system to the atmosphere, resulting in large greenhouse gas emissions. Or it can flow to the mine workings which is extremely hazardous in terms of mine fires and explosions.

This Example does not seek to build a realistic model of a specific mine. Instead, it explains how the TensorMechanics module can be used to build such a model, by exploring a very simplified and contrived 2D toy model. Of particular interest are the input parameters used and how they effect the results.

2 The model setup

A 2D model representing a transverse section of overburden above a longwall panel is studied in this Example. It is shown in Figure 2.1. The longwall panel is 300 m wide and the height of extraction is 3 m. The transverse section describes only half (150 m) of the panel and it assumed that the situation is symmetric about the panel's mid line. The panel is 400 m deep ($0 \leq z \leq 400$). The model measures 450 m in the y direction ($0 \leq y \leq 450$). The model is actually 1 m in the x direction but this is unimportant in the subsequent analysis.

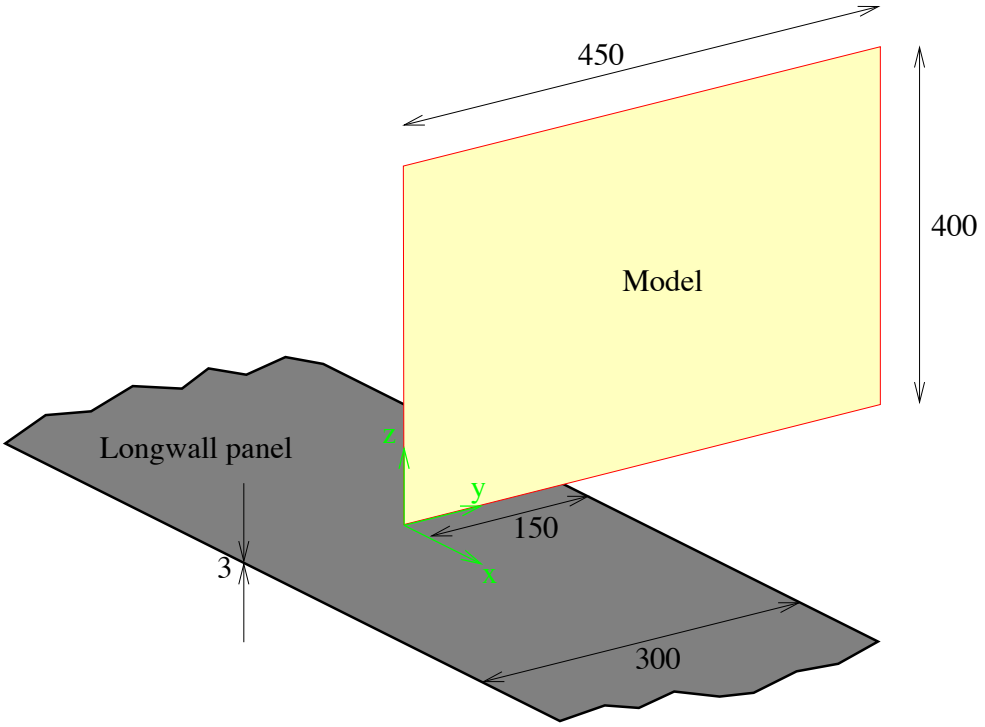

Figure 2.1: A graphic of the 2D model used in this Example. All dimensions are in metres. The geometry is described in the text.

The overburden is assumed homogeneous (but anisotropic). Boundary conditions are described below. The overburden's density is 2500 kg.m^{-3}.

3 Elastic simulations

The simulation results quoted in this section are derived using the MOOSE input file `cosserat_elastic.i`.

3.1 Motivation

Setting the strata's yield strengths very high means that the deformation is purely elastic. Of course this is unphysical, but it is interesting from a theoretical viewpoint. An example deformation is shown in Figure 3.1.

The boundary conditions in this Chapter are: roller on $y_{\min}$ and $y_{\max}$; no rotation around the x axis on $y_{\min}$; fixed on $z_{\min}$ where there is no excavation; stress-free on the top and the roof of the excavation. Therefore, the overburden is free to move vertically under the action of gravity, and this models half of an excavation that is 300 m wide.

3.2 Beam theory

The beam deformation may be compared with simple beam theory by thinking of the overburden as a beam of thickness $T = 400\,\mathrm{m}$ and length $L = 300\,\mathrm{m}$, clamped at its ends and subject to its own self load. The maximum deflection of such a beam is

$$u_z^{\max} = \frac{\rho T W g L^4}{384 E I} \ . \tag{3.1}$$

Here $\rho = 2500\,\mathrm{kg.m^{-3}}$ is the beam's density, $W = 10\,\mathrm{m}$ is its width, $g = 10\,\mathrm{m.s^{-2}}$ is gravitational acceleration, $E = 8\,\mathrm{GPa}$ is the Young's modulus of the beam, I its momenta of intertia:

$$I = \int_{-T/2}^{T/2} \mathrm{d}z \int_{-W/2}^{W/2} \mathrm{d}x z^2 = (2W/3)(T/2)^3 \ . \tag{3.2}$$

Substituting this into the formula for maximum deflection yield

$$u_z^{\max} = \frac{\rho g L^4}{32 E T^2} \approx 800/T^2 \ , \tag{3.3}$$

(measured in units of m). This formula will never give the precise displacement since various assumptions (such as the pinned end conditions, and neglecting all but the lowest-order terms) have been made in its development.

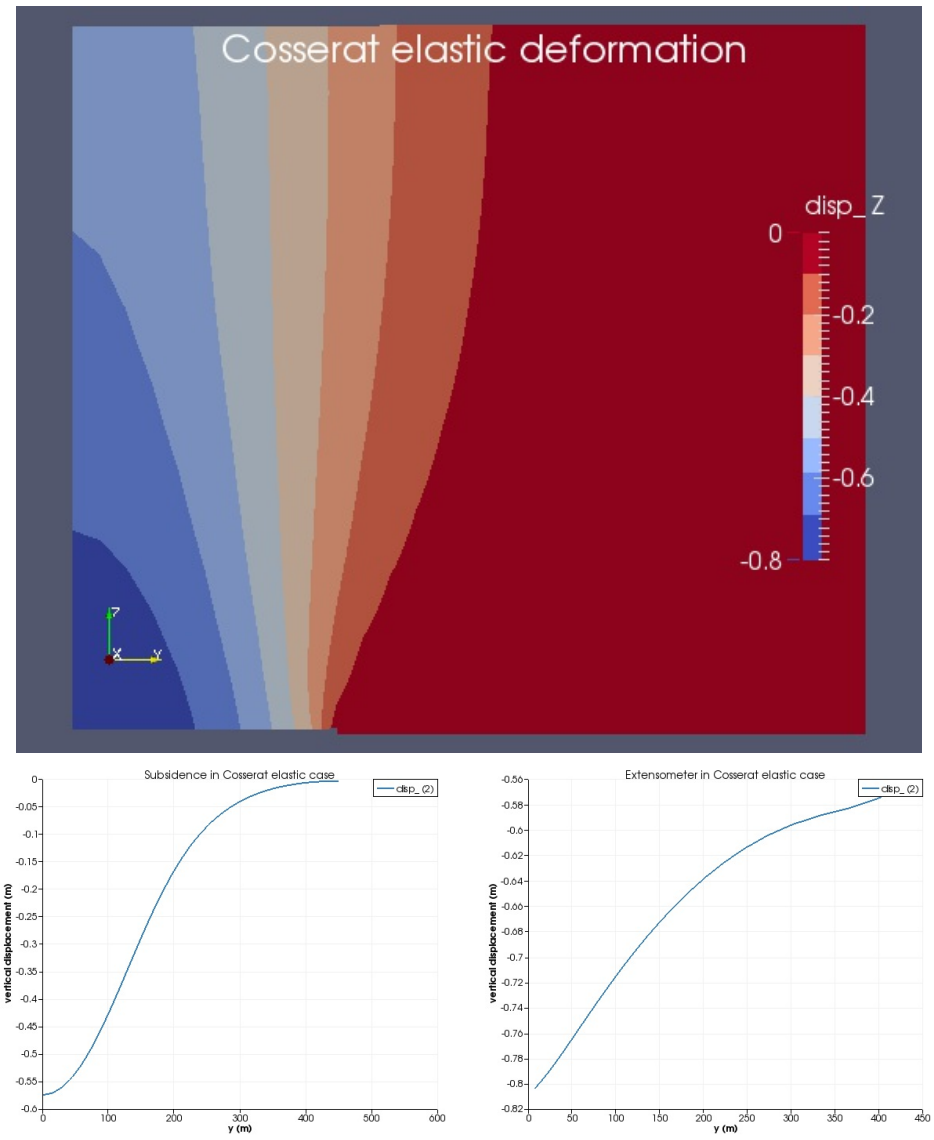

Figure 3.1: Deformation of the overburden when using Cosserat elasticity with $T_{\text{Cosserat}} = 1\,\text{m}$ and $k_{\text{shear}} = 1\,\text{GPa.m}^{-1}$. The bottom figures show "subsidence", which is vertical displacement on the top surface of the model; and "extensometer" which is vertical displacement along a vertical line that runs down the left-hand-side of the mode.

3.3 Comparison with beam theory — non-Cosserat case

Before exploring the effects of introducing Cosserat mechanics, it is useful to quantify the accuracy of Eqn (3.3) for various T, using standard (non-Cosserat) elasticity (and modifying the model described in Chapter 2 to have an overburden of thickness T instead of just $T = 400\,\mathrm{m}$). To do this, the input file `cosserat_elastic.i` is used, but the layer thickness, and Cosserat moduli are set very large. The mesh used is different in each case, but is set dense enough so that mesh dependencies are small.

T	Eqn (3.3)	MOOSE (non-Cosserat)	N
400	0.005	0.19	1000
100	0.08	0.33	1000
40	0.5	0.89	4000
10	8	8.7	20000

Table 3.1: Comparison of the approximate analytic deflection of Eqn (3.3) with MOOSE's non-Cosserat result. MOOSE's deflection is measured at the roof of the coal seam ($z = 0$). The last column, N, indicates the number of elements in the mesh before reasonable mesh-independence is obtained ($N = 1000$ was the minimum number tried).

The results are tabulated in Table 3.1. Evidently, Eqn (3.3) under-predicts the displacement for large T. This is due to the extra freedom allowed by the model compared with the pinned ends used by the theoretical development, as well as higher-order terms that are obviously present in such a thick beam. Moreover, the MOOSE displacement is always a function of z (the vertical direction) as is obvious from Figure 3.1.

3.4 Comparison with beam theory — Cosserat case

In many locations where coal seams are present, the overburden is highly stratified: it consists of layers of rock that have been deposited over time. Conceptually the rock looks like a "layer cake" of fairly uniform layers of rock separated by thin and weak horizontal "joints". Therefore, modelling the rock mass as an isotropic body is not very accurate. A better approach is to model it as a layered material, and this is accomplished by MOOSE's layered Cosserat elasticity.

Layered Cosserat elasticity allows simulation of a layered material without having to mesh each individual layer. Setting the Cosserat joint normal stiffness large and the joint shear stiffness small models a layered material in which the layers behave independently. This is described fully in the documentation for the Cosserat test suite in MOOSE. Similar results to Table 3.1 may therefore be obtained by keeping $T = 400\,\mathrm{m}$, but varying the Cosserat-layer thickness.

The results are shown in Table 3.2. It is clear that:

1. less elements are needed to obtain reasonable convergence ($N = 1000$ was the smallest number of elements used in each set of simulations) but this is offset by the increased number of degrees-of-freedom (1 in this case, and 2 in the general 3D case);

2. the deformation in the Cosserat case is larger than the standard case (because there is more freedom)

T_{Cosserat}	Eqn (3.3)	MOOSE (Cosserat)	N
400	0.005	0.31	1000
100	0.08	0.67	1000
40	0.5	1.85	4000
10	8	14.1	9000

Table 3.2: Comparison of the approximate analytic deflection of Eqn (3.3) using $T = T_{\text{Cosserat}}$ with MOOSE's layered Cosserat result with different Cosserat-layer thicknesses, T_{Cosserat}. This may be compared with Table 3.1.

3.5 The deformation in the Cosserat case with a variety of Cosserat parameters

In reality, the Cosserat joints do not have zero shear stiffness. Table 3.3 quantifies the maximum vertical displacement for a variety of physically-realistic joint shear stiffnesses and Cosserat layer thicknesses.

Comparing Tables 3.1, 3.2 and 3.3, it is clear that:

1. for large Cosserat joint stiffness (compared with $E = 8\,\text{GPa}$) the deflection is identical to the non-Cosserat case (as is expected);

2. for small Cosserat joint stiffness, the deflection approaches the limit of independent layers enumerated in Table 3.2;

3. for some intermediate values, the result is only a function of $T_{\text{Cosserat}} h_{\text{shear}}$ (as is expected from Cosserat theory).

T_{Cosserat}	k_{shear} (GPa.m^{-1})	$u_z^{\max}$	N
1	0.01	27	15000
1	0.1	3.4	4000
1	1	0.57	1000
1	10	0.23	1000
1	100	0.19	1000
10	0.01	2.9	4000
10	0.1	0.57	1000
10	1	0.23	1000
10	10	0.19	1000
10	100	0.19	1000

Table 3.3: Maximum deflection as a function of Cosserat layer thickness, T_{Cosserat} and Cosserat joint shear stiffness k_{shear}. N indicates the number of elements needed before reasonable mesh-independence is attained ($N = 1000$ was the minimum number tried).

4 Weak-plane plasticity

4.1 Introduction

In this chapter, the overburden is modelled using weak-plane plasticity in conjunction with Cosserat mechanics. The MOOSE input file used to generate the following results is `cosserat_wp_only.i`. The weak plane normal is assumed to be vertical (in the z direction. The parameters used are list in Table 4.1.

Young's modulus	8 GPa
Poisson's ratio	0.25
Cosserat layer thickness	1 m
Cosserat joint shear stiffness	1 GPa.m^{-1}
Cosserat joint normal stiffness	large
Weak-plane cohesion	0.1 MPa
Weak-plane friction angle	20 deg
Weak-plane dilation angle	10 deg
Weak-plane tensile strength	0.1 MPa
Weak-plane compressive strength	100 MPa (softening)

Table 4.1: Parameters used in the model with weak-plane plasticity. Softening for the compressive strength is used in some simulations — see text.

The mesh is kept fixed (at $N = 1000$) in the following simulations, in contrast to Chapter 3. This is rather standard practice in finite-element simulations of underground material. Usually the mesh is chosen to be fine enough so that the resolution is adequate in the region of interest, and then the mesh is fixed. This is motivated by practicalities: it is usually computationally impractical to perform many simulations with gradually finer mesh to determine the continuum limit; and the input parameters (Young's modulus, strengths, etc) are so poorly constrained by observation[1] that such a study is rather pointless anyway. The approach that is usually taken is to fix the mesh and vary the input parameters so the results (subsidence, etc) match observation.

[1]For instance, hydraulic permeabilities are usually only constrained to within a couple of orders of magnitude, and mechanical properties to within a factor of 5.

4.2 An unconstrained roof, and constraining boundary conditions

The elastic parameters in Table 4.1 match those used to generate Figure 3.1. Adding the weak-plane plasticity produces dramatically higher deformations, as shown in Figure 4.1. Such high displacements are not possible because the floor of the excavation constrains $u_z^{\max} \geq -3\,\mathrm{m}$. In fact, the floor strata "heave" — they move slightly upwards — so usually the maximum downwards displacement might be between 2.5 m and 2.9 m in the case at hand. I have found MOOSE's constraints to exhibit poor convergence in the case at hand, therefore, a prescribed boundary condition on the roof of the excavation is used in this Example.

The prescribed boundary condition takes one of two forms:

$$u_z = \begin{cases} u_z^{\max} \max\left(\min\left(\left(\frac{t}{t_{\mathrm{end}}}(y_{\max} - y_{\min}) + y_{\min} - y\right)/d_{\mathrm{closure}}, 1\right), 0\right) & \text{or} \\ u_z^{\max} \frac{t}{t_{\mathrm{end}}} \max\left(\min\left((y_{\max} - y)/d_{\mathrm{closure}}, 1\right), 0\right) \end{cases} \quad (4.1)$$

The following parameters are chosen: $u_z^{\max} = -3\,\mathrm{m}$, $y_{\min} = 0$, $y_{\max} = 150\,\mathrm{m}$ and $d_{\mathrm{closure}} = 15\,\mathrm{m}$. These two forms correspond physically to the following.

1. "Sideways excavation", where the coal is excavated from $y_{\min}$ to $y_{\max}$ during the time $0 \leq t \leq t_{\max}$. At time t, the excavation has reached $y_t = y_{\min} + t(y_{\max} - y_{\min})/t_{\mathrm{end}}$. For y less than this amount, the roof is allowed to displace a maximum of $u_{\max}^z$. For y greater than this amount, the roof has zero displacement. There is a small region between $y_t - d_{\mathrm{closure}}$ and y_t where the roof displacement is between zero and $u_z^{\max}$, but for $y < y_t - d_{\mathrm{closure}}$, $u = u_z^{\max}$.

2. "Downwards excavation". The roof is gradually lowered. At $t = 0$ the displacement is zero, while at $t = t_{\mathrm{end}}$ the displacement is equal to $u_z^{\max}$ for most of the roof. There is a small region between $y_{\max}$ and $y_{\max} - d_{\mathrm{closure}}$ where the displacement varies between zero and $u_z^{\max}$.

A quasi-static solution is sought at each timestep, and no dynamics is used, so "time" has no real physical meaning, except that it allows the roof to be gradually lowered.

For a single timestep, both "sideways" and "downwards" excavation produce the same result. This is shown in Figure 4.2.

4.3 Multiple excavation steps

However, the results are markedly different when using multiple steps. Figure 4.3 shows the displacement when using 10 steps. In the "sideways" excavation, only the bottom row of elements is actually deforming! They have very large plastic shear and tensile strain. This is not physically realistic. However, in the "downwards" excavation, there is very little dilation of the elements in the near roof, which is also probably not realistic. This is because no substantial shear failure is activated by this type of boundary condition.

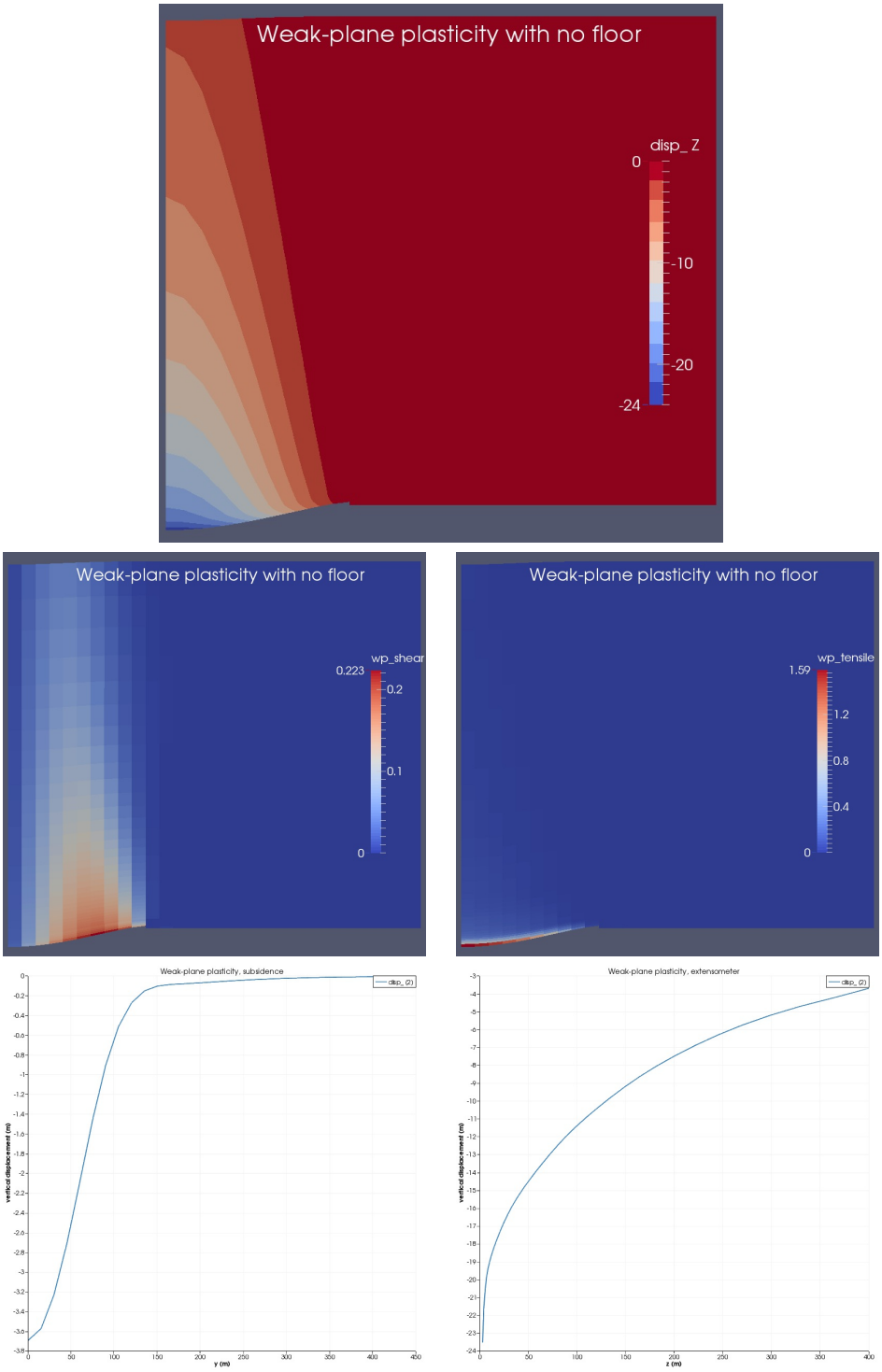

Figure 4.1: Deformation and plastic strain in the weak-plane model with no constraint on the vertical deformation of the overburden. Top: vertical displacement. Middle: shear and tensile plastic strain. Bottom: subsidence and extensometer displacement.

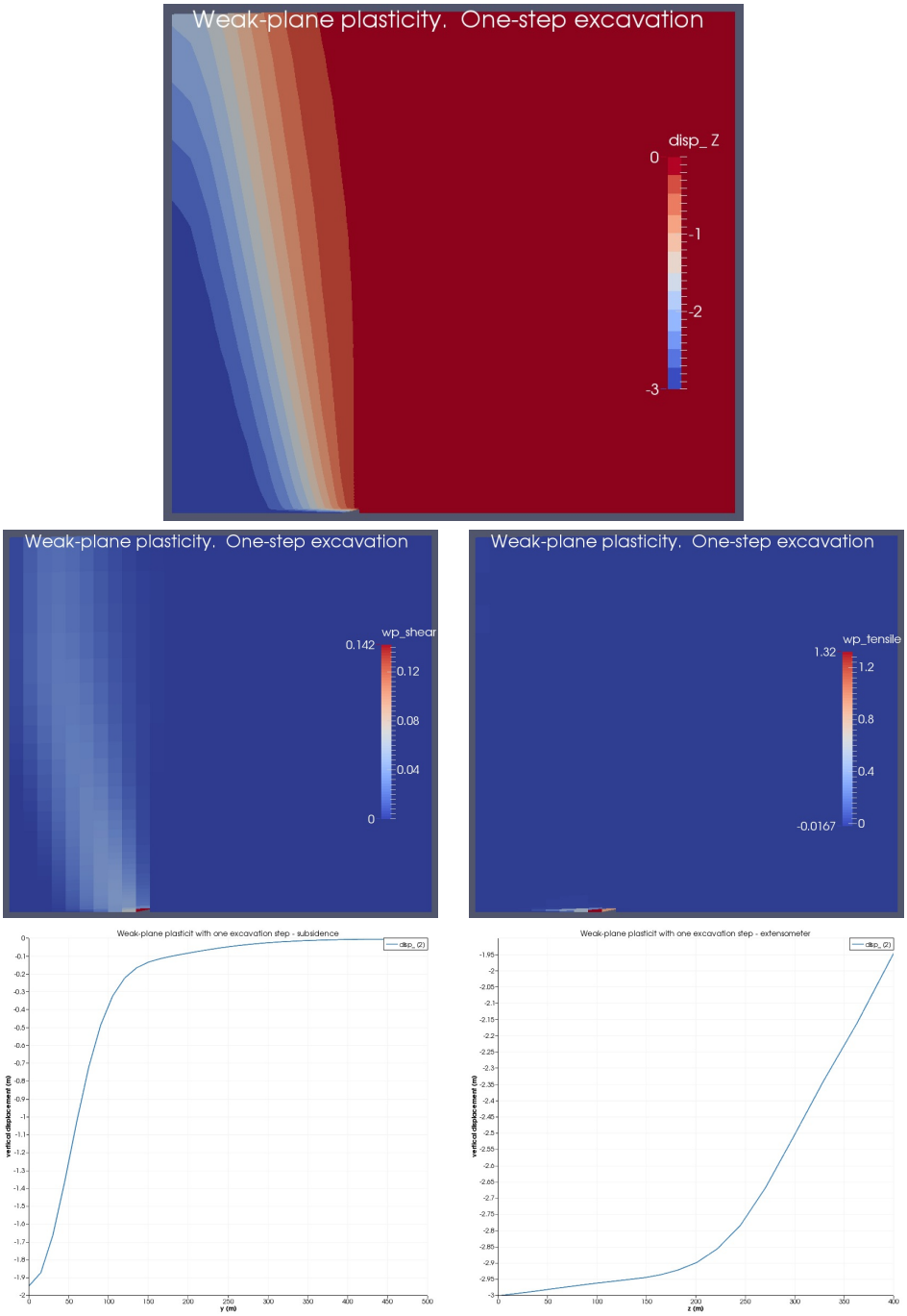

Figure 4.2: Deformation and plastic strain in the weak-plane model with $u_z^{\max} = 3\,\mathrm{m}$. The excavation is performed in one step. Top: vertical displacement. Middle: shear and tensile plastic strain. Bottom: subsidence and extensomenter displacement.

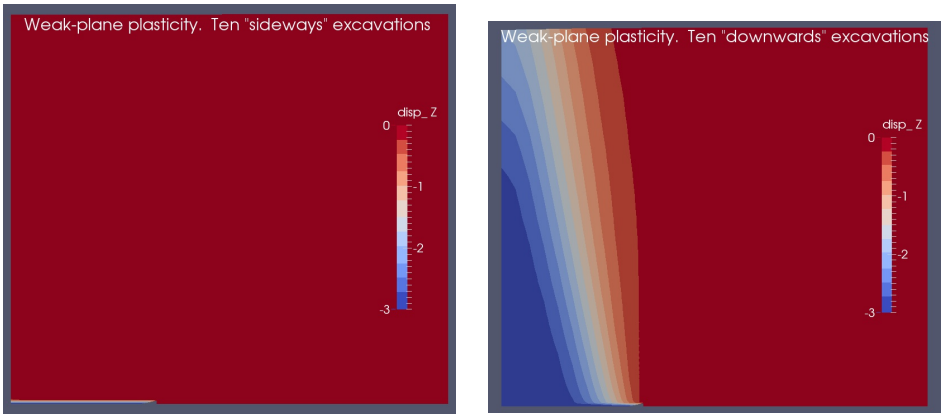

Figure 4.3: Deformation the weak-plane model when using either the "sideways" or "downwards" movement of the excavation roof.

4.4 Softening the compressive strength

Consider now an alternate plastic model with a softening weak-plane compressive strength. At zero (or negative) plastic tensile strain it is large (100 MPa), but a plastic tensile strain equal to unity it has softened all the way down to 1 MPa. Physically this corresponds to a rock then when pulled apart in tension (such as the roof being pulled downwards) it can then not withstand much compressive load, until it is recompacted somewhat. The results are shown in Figure 4.4.

4.5 Computational expense

The number of residual computations for each of the simulations mentioned above is presented in Table 4.2

Simulation	N
Unconstrained roof	209
One-step excavation	350
10-steps "sideways"	64
10-steps "downwards"	999
10-steps "sideways" with softening	501

Table 4.2: The number of residual calculations, N, for the weak-plane simulations

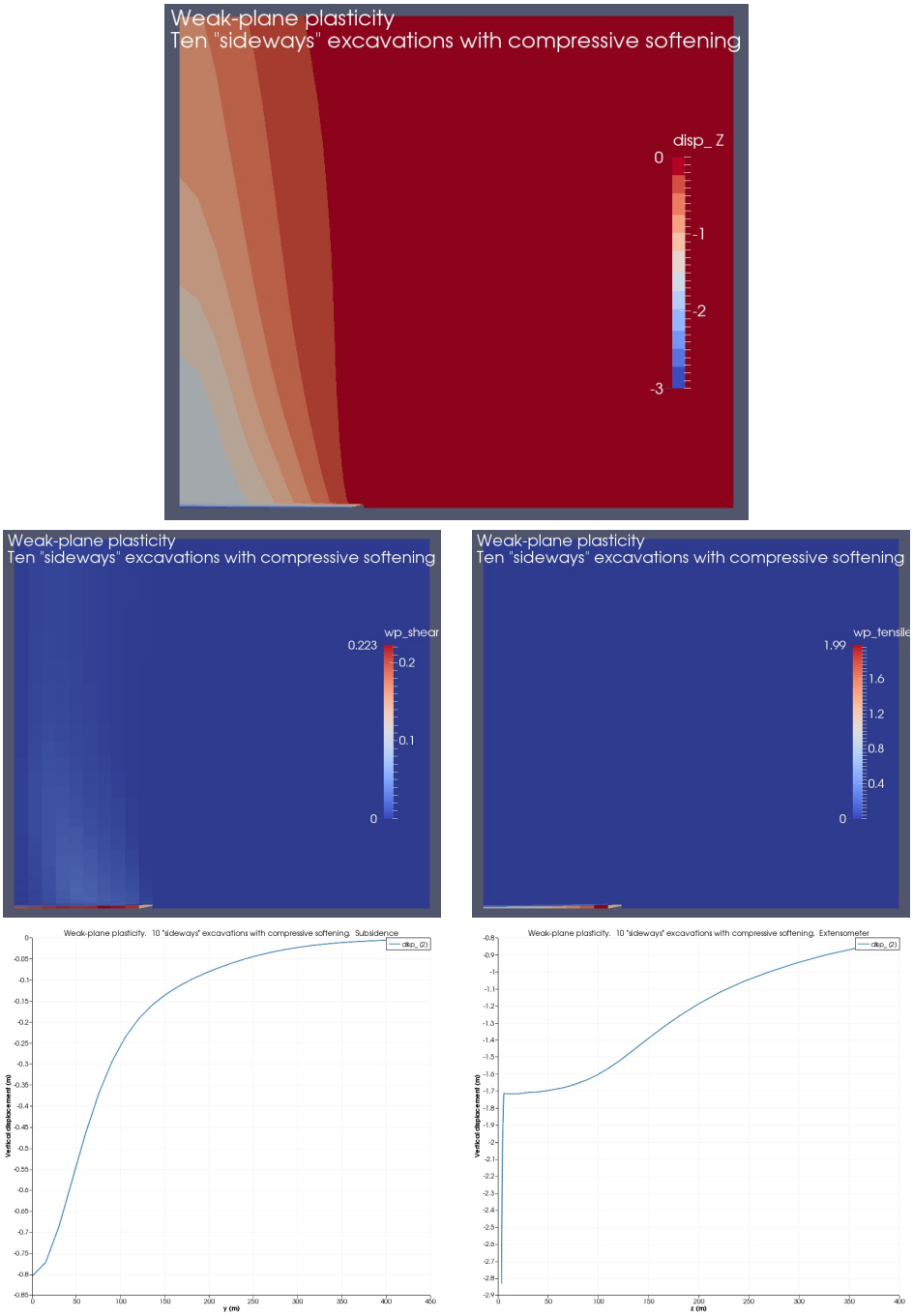

Figure 4.4: Deformation and plastic strain in the weak-plane model with $u_z^{\max} = 3\,\mathrm{m}$. The excavation is performed in 10 steps using the "sideways" scheme. The compressive strength softens from 100 MPa to 1 MPa. Top: vertical displacement. Middle: shear and tensile plastic strain. Bottom: subsidence and extensomenter displacement.

5 Weak-plane plasticity and Drucker-Prager plasticity

This will be added in the future. Illustrates the effect of rock failure via capped Drucker-Prager plasticity.

6 Capped Mohr-Coulomb plasticity

This will be added in the future. Illustrates the effect of rock failure via capped Mohr-Coulomb plasticity.

7 Porepressures

This will be added in the future. Illustrates the effect of porepressures and subsequent fluid flow.